Appendix. Supplementary material

He *et al*., Crystal versus melt compositional effects on the partitioning of the first-row transition and high field strength elements between clinopyroxene and silicic, alkaline, aluminous melts

Supplementary tables

Table S1. Experimental conditions and run products.
Table S2. Trace element compositions of starting materials in ppm, as measured by LA-ICP-MS under single-spot (30 μm) analytical mode.
Table S3. A summary of time-temperature paths for the successful experiments.
Table S4. Major element compositions of the SPI standard glass and pyroxene in wt%, as measured by EPMA.
Table S5. Major and trace element results for USGS glasses (BIR-1G, BHVO-2G, BCR-2G), MPI-DING glasses (ML3B-G, StHs6/80-G, T1-G), and the Chinese Geological Standard Glass CGSG-1 under different analytical modes by LA-ICP-MS.
Table S6. Cpx compositions in terms of molar fractions.
Table S7. Trace element (ppm) compositions of glasses, as measured by LA-ICP-MS under single-spot (30 mm) analytical mode.
Table S8. Selected major (wt% oxides) and trace (ppm) element compositions of cpx, as measured by LA-ICP-MS under different analytical modes.
Table S9. Major element (wt%) composition of coexisting cpx (along the A–B transect in Figure 1) and galss (random spot analysis) from run 9H07-2, as measured by EPMA.
Table S10. Best fits for lattice strain parameters for individual experiments.

Supplementary figures and captions

Fig. S1

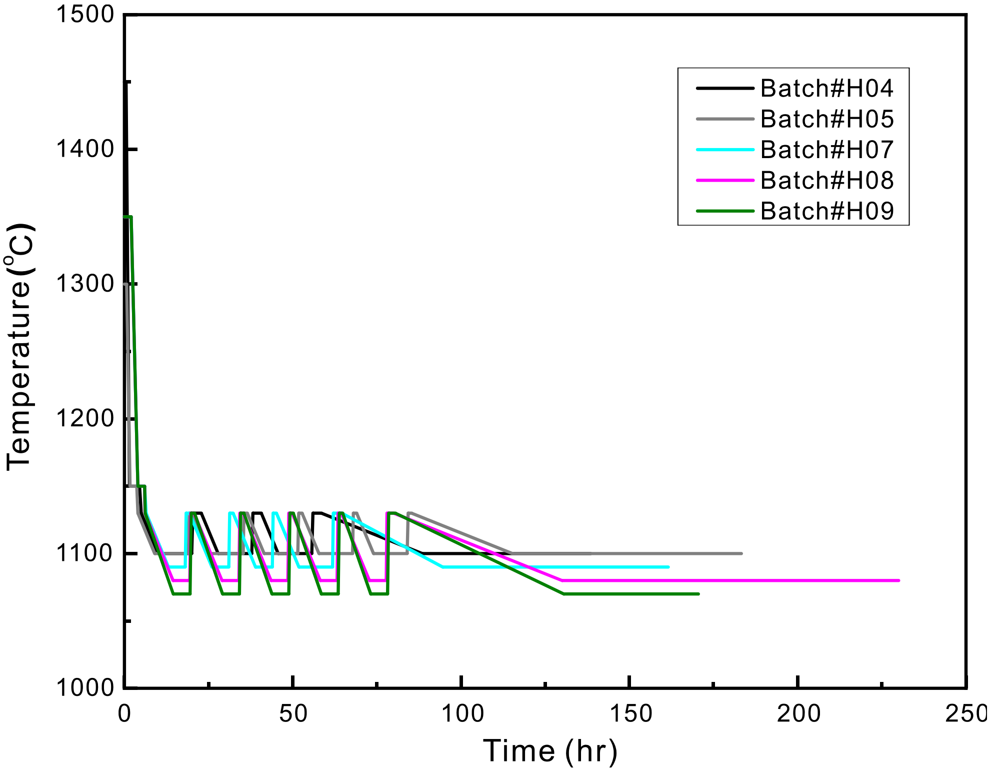

Fig. S1. Time-temperature paths for the successful experiments. For Batch#H04, runs were first heated at 1450 °C for 0.5 h, cooled and maintained at 1150 °C for 3 h; runs were then oscillated between 1100 and 1130 °C for 3 rounds with a heating and cooling rate of 90 and 6 °C/h, respectively; and the runs were finally decreased to 1100 °C at rate of 1 °C/h and maintained for 50 h. For Batch#H05, runs were first heated at 1300 °C for 40 min, cooled and maintained at 1150 °C for 2 h; runs were then oscillated between 1100 and 1130 °C for 5 rounds with a heating and cooling rate of 120 and 6 °C/h, respectively; and the runs were finally decreased to 1100 °C at rate of 1 °C/h and maintained for 68 h. For Batch#H07, runs were first heated at 1350 °C for 2 h, cooled and maintained at 1150 °C for 2 h; runs were then oscillated between 1090 and 1130 °C for 4 rounds with a heating and cooling rate of 160 and 6 °C/h, respectively; and the runs were finally decreased to 1090 °C at rate of 1.3 °C/h and maintained for 67 h. For Batch#H08, runs were first heated at 1350 °C for 2 h, cooled and maintained at 1150 °C for 2 h; runs were then oscillated between 1080 and 1130 °C for 5 rounds with a heating and cooling rate of 200 and 6 °C/h, respectively; and the runs were finally decreased to 1080 °C at rate of 1 °C/h and maintained for 100 h. For Batch#H09, runs were first heated at 1350 °C for 2 h, cooled and maintained at 1150 °C for 2 h; runs were then oscillated between 1070 and 1130 °C for 5 rounds with a heating and cooling rate of 180 and 7.2 °C/h, respectively; and the runs were finally decreased to 1070 °C at rate of 1.2 °C/h and maintained for 40 h.

Fig. S2

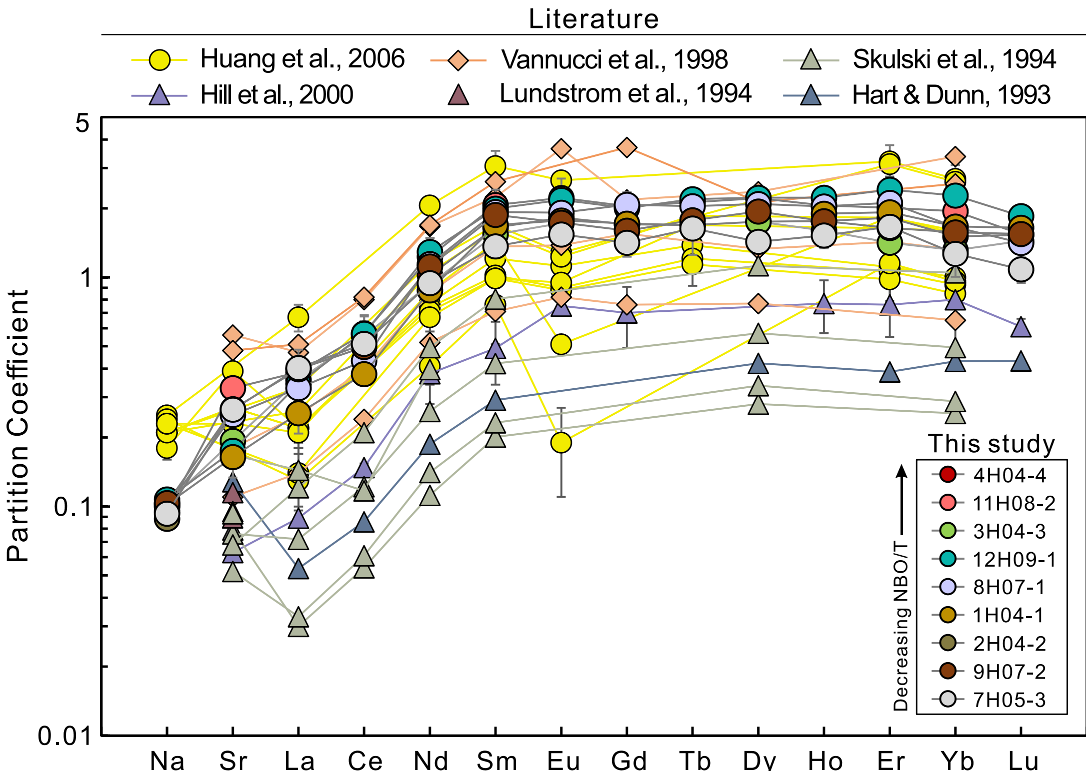

Fig. S2. Cpx–melt LILE (Na, Sr) and REE partition coefficient patterns obtained from nine representative runs with a range of melt NBO/T (0.10–0.22) in this study. The partitioning data from the literature, filtered based on diopsidic cpx with $^{iv}Al < 0.20$, are shown for comparison.

Fig. S3

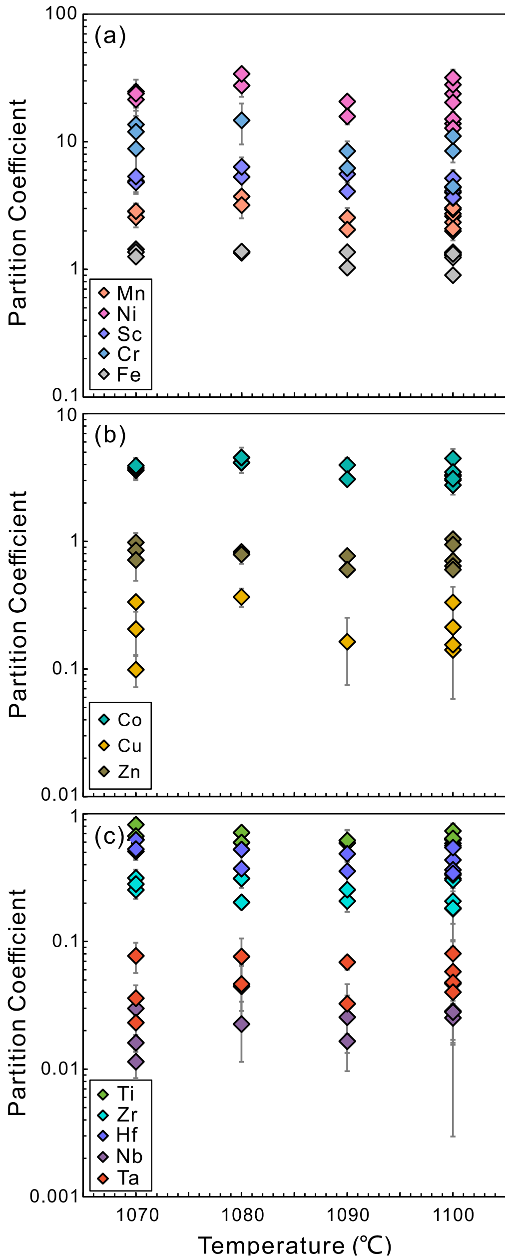

Fig. S3. Partition coefficients of (a) Mn, Ni, Sc, Cr, Fe, (b) Co, Cu, Zn, and (c) Ti, Zr, Hf, Nb, and Ta between cpx and melt as a function of equilibrium temperature.

Fig. S4

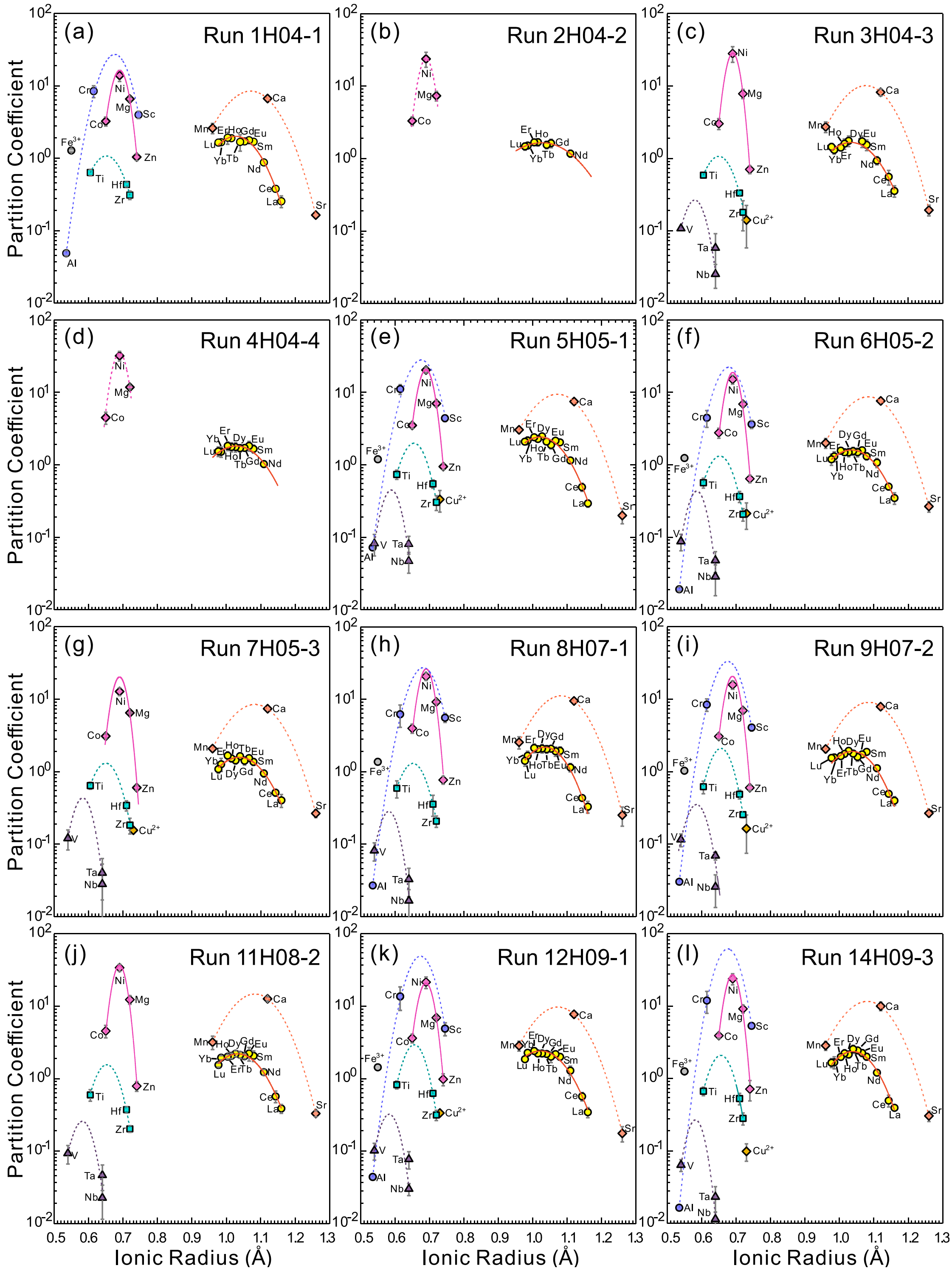

Fig. S4. Onuma diagrams showing partition coefficients for di-, tri-, tetra-, and pentavalent cations between cpx and melt as a function of ionic radii (in Å; Shannon, 1976). Ionic radii in VI- and VIII-fold coordination are taken for cations on the M1 and M2 site, respectively. The partitioning data are from 12 runs reported in this study.

Fig. S5

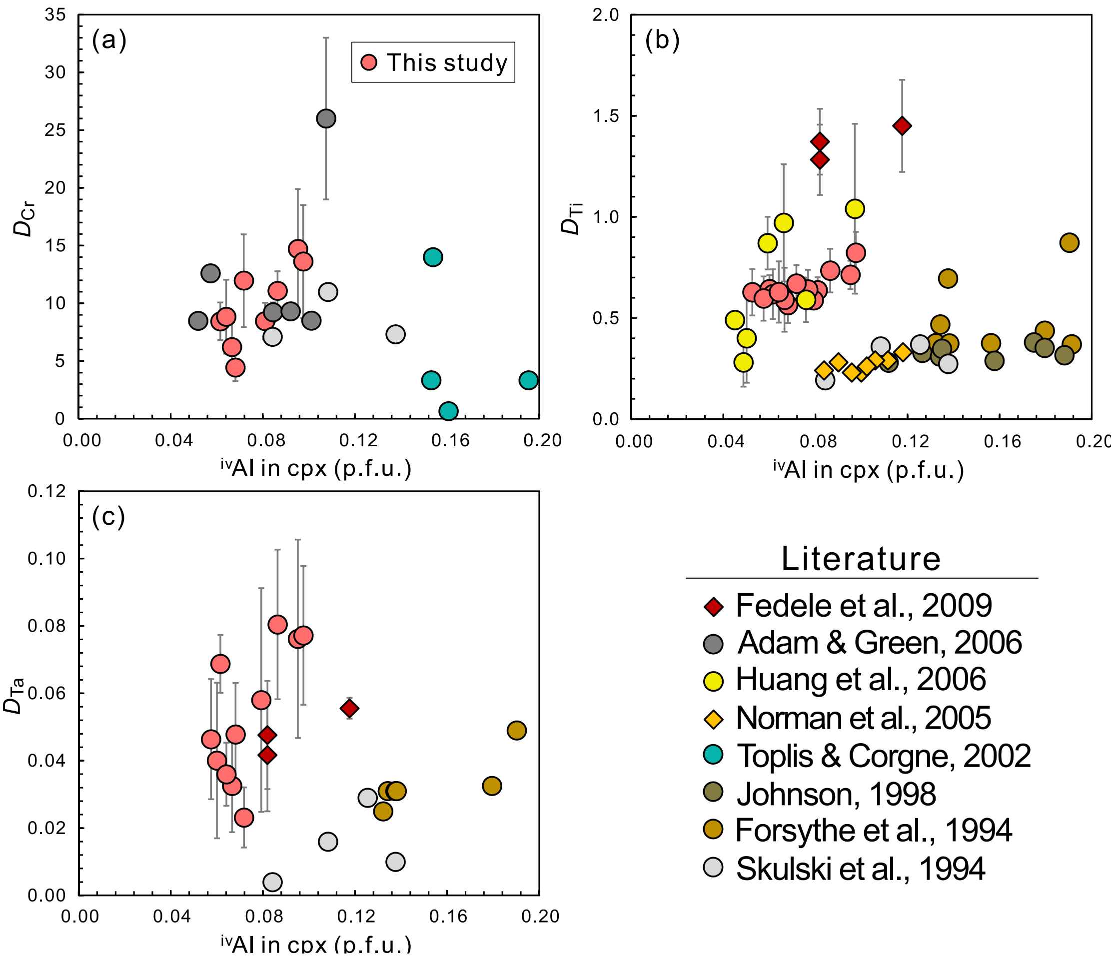

Fig. S5. Partition coefficients of (a) Cr, (b) Ti, and (c) Ta between cpx and melt as a function of ^{iv}Al content (p.f.u.) of the cpx. Other partition coefficients for diopsidic cpx with ^{iv}Al < 0.2 from the literature are shown for comparison.

Fig. S6

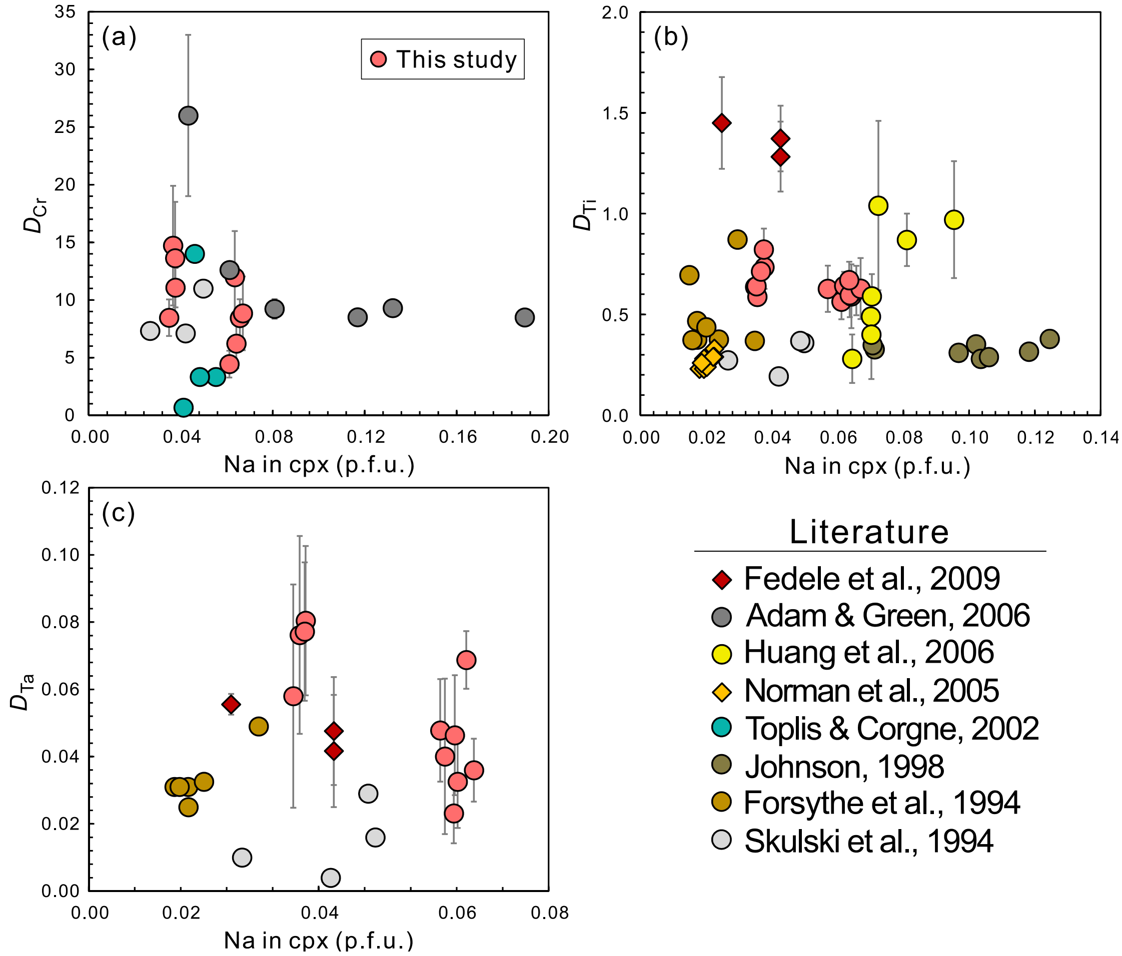

Fig. S6. Partition coefficients of (a) Cr, (b) Ti, and (c) Ta between cpx and melt as a function of Na content (p.f.u.) of the cpx. Other partition coefficients for diopsidic cpx with $^{iv}Al < 0.2$ from the literature are shown for comparison.

References

Adam, J., and Green, T. (2006) Trace element partitioning between mica- and amphibole-bearing garnet lherzolite and hydrous basanitic melt: 1. Experimental results and the investigation of controls on partitioning behaviour. Contributions to Mineralogy and Petrology, 152, 1-17.

Fedele, L., Zanetti, A., Morra, V., Lustrino, M., Melluso, L., and Vannucci, R. (2009) Clinopyroxene/liquid trace element partitioning in natural trachyte–trachyphonolite systems: Insights from Campi Flegrei (southern Italy). Contributions to Mineralogy and Petrology, 158, 337-356.

Forsythe, L.M., Nielsen, R.L., and Fisk, M.R. (1994) High-field-strength element partitioning between pyroxene and basaltic to dacitic magmas. Chemical Geology, 117, 107-125.

Hart, S.R., and Dunn, T. (1993) Experimental cpx/melt partitioning of 24 trace elements. Contributions to Mineralogy and Petrology, 113, 1-8.

Hill, E., Wood, B.J., and Blundy, J.D. (2000) The effect of Ca-Tschermaks component on trace element partitioning between clinopyroxene and silicate melt. Lithos, 53, 203-215.

Huang, F., Lundstrom, C., and McDonough, W. (2006) Effect of melt structure on trace-element partitioning between clinopyroxene and silicic, alkaline, aluminous melts. American Mineralogist, 91, 1385-1400.

Johnson, K.T.M. (1998) Experimental determination of partition coefficients for rare earth and high-field-strength elements between clinopyroxene, garnet, and basaltic melt at high pressures. Contributions to Mineralogy and Petrology, 133, 60-68.

Lundstrom, C.C., Shaw, H.F., Ryerson, F.J., Phinney, D.L., Gill, J.B., and Williams, Q. (1994) Compositional controls on the partitioning of U, Th, Ba, Pb, Sr and Zr between clinopyroxene and haplobasaltic melts: implications for uranium series disequilibria in basalts. Earth and Planetary Science Letters, 128, 407-423.

Morimoto, N. (1988) Nomenclature of pyroxenes. Mineralogy and Petrology, 39, 55-76.

Norman, M., Garcia, M.O., and Pietruszka, A.J. (2005) Trace-element distribution coefficients for pyroxenes, plagioclase, and olivine in evolved tholeiites from the 1955 eruption of Kilauea Volcano, Hawai', and petrogenesis of differentiated rift-zone lavas. American Mineralogist, 90, 888-899.

Shannon, R. D. (1976) Revised effective ionic radii and systematic studies of interatomic distances in halides and chalcogenides. Acta Crystallographica, A32, 751–767.

Skulski, T., Minarik, W., and Watson, E.B. (1994) High-pressure experimental trace-element partitioning between clinopyroxene and basaltic melts. Chemical Geology, 117, 127-147.

Toplis, M.J., and Corgne, A. (2002) An experimental study of element partitioning between magnetite, clinopyroxene and iron-bearing silicate liquids with particular emphasis on vanadium. Contributions to Mineralogy and Petrology, 144, 22-37.

Vannucci, R., Bottazzi, P., Wulff-Pedersen, E., and Neumann, E.-R. (1998) Partitioning of REE, Y, Sr, Zr and Ti between clinopyroxene and silicate melts in the mantle under La Palma (Canary Islands): implications for the nature of the metasomatic agents. Earth and Planetary Science Letters, 158, 39-51.